

Residual Data-Driven Variational Multiscale Reduced Order Models for Parameter Dependent Problems

B. Koc, T. Chacón Rebollo, T. Iliescu

Abstract

Over the last decade, several closure modeling strategies for reduced order models (ROMs) of turbulent flows have been developed. These closure models aim to include the effect of the discarded ROM basis functions, which can significantly increase the ROM accuracy in under-resolved, turbulent flows. Probably the most active area of research in this field has been data-driven closure modeling, in which available data is used to construct accurate ROM closure operators. Most of the current data-driven ROM closures depend on the ROM coefficients. In this paper, we propose a different strategy: the ROM closure model depends on the ROM residual. We illustrate the new residual-based data-driven ROM closure within the variational multiscale (VMS) framework and investigate it in the numerical simulation of a one-dimensional parameter-dependent convection-diffusion problem. For comparison purposes, we also investigate a streamline-upwind Petrov-Galerkin (SUPG) ROM stabilization strategy and the standard Galerkin ROM (G-ROM). Our numerical investigation shows that the new residual-based data-driven VMS-ROM is more accurate than both the standard G-ROM and the SUPG-ROM.

Keywords: Reduced order models, variational multiscale, data-driven modeling, residual term, consistent model.

1 Introduction

In this paper, we investigate the modeling of sub-scale components of proper orthogonal decomposition reduced order models (POD-ROMs) of convection-dominated flows. We find our primary motivation in the low decay of the POD eigenvalues for high-Reynolds number, turbulent flows. As a consequence, the POD-ROM solution of these flows needs reduced spaces of very high dimension, incurring a high computational cost and yielding no gain with respect to full order models (FOMs), i.e., computational models obtained with classical numerical methods (e.g., finite element (FE) method).

As in the FOM case, the issue of ROM sub-scale component modeling for convection-dominated flows is closely related to the stabilization of ROMs. This is due to the diffusive effect of the sub-grid scales on the resolved scales [6]. This diffusive effect has been leveraged in constructing ROM stabilized models. In this paper, we propose a new residual-based data-driven VMS-ROM closure framework, and we compare it with both the SUPG-ROM stabilization strategy and the standard G-ROM.

A survey of VMS-ROM closure modeling is performed in Section IV.A.5 of [1]. Next, we outline several VMS-ROM closure models relevant to the new residual-based data-driven VMS-ROM closure framework. In [2], a residual-based VMS model is proposed as a ROM stabilization strategy. A two-scale VMS-ROM equipped with time-dependent orthogonal sub-grid scales is developed in [15]. A VMS-ROM closure that includes an artificial viscosity added only to the small resolved scales of the gradient is proposed in

[9]. Numerical tests in [9] show the increased numerical stability and accuracy of the VMS-ROM over the standard G-ROM and illustrate the theoretical convergence rates. In particular, a problem displaying shock-like phenomena is considered (2D traveling wave) at a moderate Péclet number ($\nu = 10^{-4}$). In [10], the VMS-ROM is extended and studied for the incompressible Navier-Stokes equations.

The SUPG-ROM strategy [2, 7, 11, 13] is one of the most popular ROM stabilization techniques. Next, we briefly mention SUPG-ROM approaches relevant to the SUPG-ROM used in our numerical investigation. In [7], the authors present an SUPG-ROM based on POD, which is investigated theoretically and numerically for the convection-diffusion equation. In this context, it is stressed that for convection-dominated problems whose solutions have a steep internal layer, using a stabilized discretization is necessary when using relatively coarse meshes. We note that, in practical applications, FE meshes are significantly coarser than the width of the internal layers. Relying on the SUPG-FEM [3], in [7], the authors use both offline and online stabilization procedures to deal with the numerical instabilities of the Galerkin method in both the FOM and the ROM. We note that the SUPG-ROM involves the full residual, thus being fully consistent. The study of appropriate choices of the SUPG-ROM stabilization parameter is considered in [7]. Two approaches are used: one based on the underlying FE discretization and the other based on the POD truncation. Thus, the question of whether the stabilization parameter should depend on the spatial resolution of the underlying FE space or on the number of POD modes used is treated in [7] by means of numerical analysis arguments. Another SUPG-ROM strategy is considered in [4], where the authors propose and numerically investigate an SUPG-ROM stabilization method for the convection term, together with a stabilization approach for the pressure term.

In this paper, we perform a systematic numerical study of the different sub-scale modeling strategies to increase the ROM accuracy for convection-dominated problems. We consider three different approaches: (i) a novel residual-based data-driven VMS-ROM (R-D2-VMS-ROM); (ii) the standard coefficient-based data-driven VMS-ROM (C-D2-VMS-ROM) [12, 17]; and (iii) a data-driven SUPG-ROM. The first two approaches are closure models, whereas the third is a stabilization method. We also note that all three approaches are data-driven approaches in which a least squares problem is solved in the offline stage to determine the closure operators (for the first two approaches) and the stabilization parameter (in the third approach) that are optimal with respect to the FOM data. Our numerical investigation shows that the new R-D2-VMS-ROM yields the most accurate results.

The outline of the paper is as follows: In section 2, we briefly outline G-ROM for the parameter-dependent convection-diffusion problem. Section 3 describes the small-large scale decomposition that underpins the VMS-ROM framework. Section 4 presents the new residual-based data-driven variational multiscale ROM (R-D2-VMS-ROM) and compare it with the standard coefficient-based D2-VMS-ROMs (C-D2-VMS-ROM). In Section 5, we outline the SUPG-ROM and list different options for the stabilization parameter. In Section 6, we provide a numerical investigation of four models: R-D2-VMS-ROM, C-D2-VMS-ROM, SUPG-ROM, and G-ROM. Section 7 concludes the paper by presenting a short summary and future research directions.

2 Galerkin Reduced Order Model (G-ROM)

To construct and test the ROMs, we use one-dimensional parameter-dependent convection-diffusion (CD) problem:

$$\begin{cases} -\mu\partial_{xx}u + c\partial_xu = f & \text{for } x \in [0, 1], \\ u(0) = 0 & \text{and } u(1) = 0, \end{cases} \quad (1)$$

where $f(x) = -c$, u , and μ represent the forcing term (c is the velocity field), the variable of interest, and the diffusion coefficient, respectively.

The Galerkin ROM (G-ROM) is one of the most common types of ROMs for fluid flows. In Algorithm 1, we outline the G-ROM construction.

Algorithm 1 Galerkin ROM (G-ROM)

- 1: Use available FOM data to construct dominant modes $\{\varphi_1, \dots, \varphi_L\}$, $L \ll d$ (where d is the dimension of the input dataset) that correspond to the largest relative kinetic energy content and represent the recurrent spatial structures of the given test problem;
 - 2: Construct a ROM approximation \mathbf{u}_L in (4) as a linear combination of ROM basis functions φ_i with ROM coefficients $(\mathbf{a}_L)_i$, i.e., $\mathbf{u}_L(x, \mu) = \sum_{i=1}^L (\mathbf{a}_L(\mu))_i \varphi_i(x)$;
 - 3: Replace \mathbf{u} in the given test problem with the ROM solution \mathbf{u}_L constructed in step 2;
 - 4: Use the Galerkin projection, which projects the resulting system in step 3 onto the ROM space \mathbf{X}^L spanned by $\{\varphi_1, \dots, \varphi_L\}$.
-

By using Algorithm 1 for the CD problem (1), we obtain the following G-ROM:

$$\mathbf{A}_{LL} \mathbf{a}_L = \mathbf{b}_L, \quad (2)$$

where the ROM operators are the matrix $(\mathbf{A}_{LL})_{ij} := \mu(\partial_x \varphi_j, \partial_x \varphi_i) + (c \partial_x \varphi_j, \varphi_i)$ and the vector $(\mathbf{b}_L)_i := (\mathbf{f}, \varphi_i)$, and \mathbf{a}_L is the vector of G-ROM coefficients, which needs to be determined.

3 Variational Multiscale Reduced Order Model (VMS-ROM)

In this section, we construct the VMS-ROM framework, which will be used in the next section to build data-driven VMS-ROMs.

First, we note that when all the ROM modes are used to create a ROM solution, the ROM approximation reads

$$\mathbf{u}_d = \sum_{i=1}^d (\mathbf{a}_d)_i \varphi_i. \quad (3)$$

In this case, \mathbf{u}_d is the most accurate ROM approximation of the FOM solution with the given data.

For laminar flows, using a few ($L \ll d$) ROM basis functions is enough to capture the main dynamics of the given problem. In other words, a low-dimensional ROM solution \mathbf{u}_L ,

$$\mathbf{u}_L = \sum_{i=1}^L (\mathbf{a}_L)_i \varphi_i, \quad (4)$$

yields an accurate approximation of the FOM solution.

However, for turbulent flow, the low-dimensional ROM solution (4) is not an accurate approximation of the FOM solution. To increase the accuracy of the L -dimensional ROM solution 4, we roughly have two options: (i) increase the G-ROM dimension, L , or (ii) add a low-dimensional closure term to the G-ROM. In this paper, we aim to increase the numerical accuracy without significantly increasing the computational cost. Thus, we choose the second option. Next, we explain what ROM closure modeling is and how it is performed in a VMS setting.

The orthogonality of the ROM basis functions allows us to decompose the total ROM space as follows: $\mathbf{X}^d = \mathbf{X}^L \oplus \mathbf{X}^S$, where $\mathbf{X}^d := \text{span}\{\varphi_1, \dots, \varphi_d\}$, $\mathbf{X}^L := \text{span}\{\varphi_1, \dots, \varphi_L\}$, and $\mathbf{X}^S := \text{span}\{\varphi_{L+1}, \dots, \varphi_d\}$. By using the same decomposition, we define the large and sub-scale solutions of the most accurate ROM solution, \mathbf{u}^d , as follows:

$$\mathbf{u}_L := \sum_{i=1}^L (\mathbf{a}_L)_i \varphi_i, \quad (5a)$$

$$\mathbf{u}_S := \sum_{i=L+1}^d (\mathbf{a}_S)_i \varphi_i. \quad (5b)$$

The most accurate ROM approximation in (3), \mathbf{u}^d , solves the following bilinear-linear form of the CD problem (1)

$$a(\mathbf{u}^d, \mathbf{v}^d) = \langle \mathbf{f}, \mathbf{v}^d \rangle, \quad \forall \mathbf{v}^d \in \mathbf{X}^d, \quad (6)$$

where the bilinear form $a(\mathbf{u}^d, \mathbf{v}^d) := -\mu \langle \partial_{xx} \mathbf{u}^d, \mathbf{v}^d \rangle + \langle c \partial_x \mathbf{u}^d, \mathbf{v}^d \rangle$, and $\langle \cdot, \cdot \rangle$ represents the L^2 inner product. By using the variational multiscale decomposition and choosing $\mathbf{v}_L = \varphi_L \in \mathbf{X}^L$ and $\mathbf{v}_S = \varphi_S \in \mathbf{X}^S$ ($\mathbf{v}^d = \mathbf{v}_L + \mathbf{v}_S$), we can decompose (6) into two problems as follows:

$$a(\mathbf{u}_L, \varphi_L) = \langle \mathbf{f}, \varphi_L \rangle - a(\mathbf{u}_S, \varphi_L) = \langle \text{Res}(\mathbf{u}_S), \varphi_L \rangle := \text{Res}_L(\mathbf{u}_S), \quad (7a)$$

$$a(\mathbf{u}_S, \varphi_S) = \langle \mathbf{f}, \varphi_S \rangle - a(\mathbf{u}_L, \varphi_S) = \langle \text{Res}(\mathbf{u}_L), \varphi_S \rangle := \text{Res}_S(\mathbf{u}_L), \quad (7b)$$

where $\text{Res}(\mathbf{u}) = \mathbf{f} - (-\mu \partial_{xx} \mathbf{u} + c \partial_x \mathbf{u})$. The matrix-vector forms of (7a)-(7b) are as follows:

$$\mathbf{A}_{LL} \mathbf{a}_L + \mathbf{A}_{LS} \mathbf{a}_S = \mathbf{b}_L, \quad (8a)$$

$$\mathbf{A}_{SL} \mathbf{a}_L + \mathbf{A}_{SS} \mathbf{a}_S = \mathbf{b}_S, \quad (8b)$$

where the matrices and the vectors are defined as follows:

$$\begin{aligned} \mathbf{A}_{ij} &= \mu \mathbf{S}_{ij} + c \mathbf{C}_{ij}, \\ \mathbf{b}_i &= \langle \mathbf{f}, \varphi_i \rangle, \\ \mathbf{S}_{ij} &= \mu \langle \partial_x \varphi_i, \partial_x \varphi_j \rangle, \\ \mathbf{C}_{ij} &= c \langle \partial_x \varphi_i, \varphi_j \rangle, \end{aligned} \quad (9)$$

where i, j could be either L or S .

4 Data-Driven Variational Multiscale ROM (D2-VMS-ROM)

In this section, we present two different types of D2-VMS-ROMs. Specifically, in Sections 4.1 and 4.2, we present the standard coefficient-based D2-VMS-ROM (C-D2-VMS-ROM) and the new residual-based D2-VMS-ROM (R-D2-VMS-ROM), respectively.

4.1 Coefficient-Based Data-Driven Variational Multiscale ROM (C-D2-VMS-ROM)

In this method, we use a linear ansatz to model the sub-scale contribution in (8a), $\mathbf{A}_{LS} \mathbf{a}_S$, as a function of the vector of large-scale ROM coefficients, \mathbf{a}_L . In (10a) and (11a), we consider two different ansatzes, which yield two different coefficient-based D2-VMS-ROMs:

$$\mathbf{A}_{LS} \mathbf{a}_S \approx \mathbf{Ansatz}(\mathbf{a}_L) = \tilde{\mathbf{A}} \mathbf{a}_L, \quad (10a)$$

$$\mathbf{C1-ROM} : (\mathbf{A}_{LL} + \tilde{\mathbf{A}}) \mathbf{a}_L = \mathbf{b}_L. \quad (10b)$$

$$\mathbf{A}_{LS} \mathbf{a}_S \approx \mathbf{Ansatz}(\mathbf{a}_L) = \tilde{\mathbf{A}} \mathbf{a}_L + \tilde{\mathbf{b}}, \quad (11a)$$

$$\mathbf{C2-ROM} : (\mathbf{A}_{LL} + \tilde{\mathbf{A}}) \mathbf{a}_L = \mathbf{b}_L - \tilde{\mathbf{b}}. \quad (11b)$$

The expectation is that the C2-D2-VMS-ROM yields more accurate results than the C1-D2-VMS-ROM since the ansatz in the C2-D2-VMS-ROM has more flexibility, i.e., it contains the D2 operator $\tilde{\mathbf{b}}$, whereas the C1-D2-VMS-ROM does not.

For both cases, to construct the D2 operators in (10b) and (11b), we need to solve the following generalized minimization problem:

$$\min_{\text{D2 operators}} \sum_{j=1}^M \left\| \mathbf{A}_{LS} \mathbf{a}_S^j - \mathbf{Ansatz}(\mathbf{a}_L^j) \right\|_{L^2}^2, \quad (12)$$

where M represents the number of parameter values used to generate the FOM data utilized in the ROM basis construction. After solving (12) for the D2 operators $\tilde{\mathbf{A}}$ and $\tilde{\mathbf{b}}$ for the ansatzes (10a) and (11a), and plugging them into (8a), we get the C1-ROM as (10b) and C2-ROM as (11b).

4.2 Residual-Based Data-Driven Variational Multiscale ROM (R-D2-VMS-ROM)

In this section, we propose two different residual-based D2-VSM-ROM (R-D2-VMS-ROM) techniques. In the first technique, we use only one ansatz to model the sub-scales in (8a), \mathbf{a}_S , as a function of the residual term $Res_S(\mathbf{a}_L)$, which is constructed by using the information from (8b). We call this model R1-D2-VMS-ROM. In the second technique, we use two ansatzes to model two closure terms; we call this method R2-D2-VMS-ROM. The first ansatz in R2-D2-VSM-ROM is constructed the same way as the ansatz in R1-D2-VSM-ROM. The second ansatz in R2-D2-VMS-ROM models $Res_L(\mathbf{a}_S)$ by using $Res_L(\mathbf{a}_S^{approx})$, which is computed in either (13a) or (14a).

For both R1-D2-VMS-ROM and R2-D2-VMS-ROM, since their construction is based on both (8a) and (8b), the expectation is that these models are more flexible than C-D2-VMS-ROM. Depending on how we model the sub-scales, in other words, how we construct the ansatz, we present four different R-D2-VMS-ROMs.

The following two R1-D2-VMS-ROM variants are obtained using only one ansatz to model the sub-scales, \mathbf{a}_S , as follows:

$$\mathbf{a}_S \approx \mathbf{Ansatz}(Res_S(\mathbf{a}_L)) = \tilde{\mathbf{A}} Res_S(\mathbf{a}_L), \quad (13a)$$

$$\mathbf{R1a-ROM} : (\mathbf{A}_{LL} - \mathbf{A}_{LS} \tilde{\mathbf{A}} \mathbf{A}_{SL}) \mathbf{a}_L = \mathbf{b}_L - \mathbf{A}_{LS} \tilde{\mathbf{A}} \mathbf{b}_S. \quad (13b)$$

$$\mathbf{a}_S \approx \mathbf{Ansatz}(Res_S(\mathbf{a}_L)) = \tilde{\mathbf{A}} Res_S(\mathbf{a}_L) + \tilde{\mathbf{b}}, \quad (14a)$$

$$\mathbf{R1b-ROM} : (\mathbf{A}_{LL} - \mathbf{A}_{LS} \tilde{\mathbf{A}} \mathbf{A}_{SL}) \mathbf{a}_L = \mathbf{b}_L - \mathbf{A}_{LS} \tilde{\mathbf{A}} \mathbf{b}_S - \mathbf{A}_{LS} \tilde{\mathbf{b}}, \quad (14b)$$

where the residual term is defined as $Res_S(\mathbf{a}_L) := (\mathbf{b}_S - \mathbf{A}_{SL} \mathbf{a}_L)$. The main difference between the ansatzes in (13a) and (14a) is the D2 operator $\tilde{\mathbf{b}}$. Since R-D2-VMS-ROM, which is a consistent model, is constructed using the residual term to model the sub-scales, we do not expect that adding a vector term in the ansatz yields results that are very different from the case in which we do not add a vector term. To ensure a fair comparison of these two methods, in the numerical results section, we provide the consistency error tables to determine whether the vector $\tilde{\mathbf{b}}$ is needed.

For both cases, to construct the D2 operators in (13b) and (14b), we need to solve the following generalized minimization problem:

$$\min_{\text{D2 operators}} \sum_{j=1}^M \left\| \mathbf{a}_S^j - \mathbf{Ansatz}(Res_S(\mathbf{a}_L^j)) \right\|_{L^2}^2. \quad (15)$$

After solving (15) for the D2 operators $\tilde{\mathbf{A}}$ and $\tilde{\mathbf{b}}$ for the ansatzes (13a) and (14a), and plugging them into (8a), we get the models R1a-ROM (13b) and R1b-ROM (14b).

Next, we present two more R-D2-VM-ROM variants. The main difference between these models and those presented above is that the latter have much more information related to the sub-scales since they gradually model the sub-scales. The first ansatz in (16a) and (17a) is constructed to approximate the sub-scales by using the large scale residual, which is projected onto the sub-scales. The second ansatz is used to approximate the sub-scales residual, which is projected onto the large scales by using the approximated sub-scales, which in turn are solved from the first ansatz:

$$\mathbf{a}_S \approx \mathbf{Ansatz1}(Res_S(\mathbf{a}_L)) = \tilde{\mathbf{A}}_1 Res_S(\mathbf{a}_L), \quad (16a)$$

$$Res_L(\mathbf{a}_S) \approx \mathbf{Ansatz2}(Res_L(\mathbf{a}_S^{approx})) = \tilde{\mathbf{A}}_2 Res_L(\mathbf{a}_S^{approx}), \quad (16b)$$

$$\mathbf{R2a-ROM} : (\mathbf{A}_{LL} - \tilde{\mathbf{A}}_2 \mathbf{A}_{LS} \tilde{\mathbf{A}}_1 \mathbf{A}_{SL}) \mathbf{a}_L = \tilde{\mathbf{A}}_2 (\mathbf{b}_L - \mathbf{A}_{LS} \tilde{\mathbf{A}}_1 \mathbf{b}_S). \quad (16c)$$

$$\mathbf{a}_S \approx \mathbf{Ansatz1}(Res_S(\mathbf{a}_L)) = \tilde{\mathbf{A}}_1 Res_S(\mathbf{a}_L) + \tilde{\mathbf{b}}_1, \quad (17a)$$

$$Res_L(\mathbf{a}_S) \approx \mathbf{Ansatz2}(Res_L(\mathbf{a}_S^{approx})) = \tilde{\mathbf{A}}_2 Res_L(\mathbf{a}_S^{approx}) + \tilde{\mathbf{b}}_2, \quad (17b)$$

$$\mathbf{R2b-ROM} : (\mathbf{A}_{LL} - \tilde{\mathbf{A}}_2 \mathbf{A}_{LS} \tilde{\mathbf{A}}_1 \mathbf{A}_{SL}) \mathbf{a}_L = \tilde{\mathbf{A}}_2 \left[\mathbf{b}_L - \mathbf{A}_{LS} (\tilde{\mathbf{A}}_1 \mathbf{b}_S + \tilde{\mathbf{b}}_1) \right] + \tilde{\mathbf{b}}_2. \quad (17c)$$

$$\min_{\text{D2 operators}} \sum_{j=1}^M \left\| Res_L(\mathbf{a}_S^j) - \mathbf{Ansatz2}(Res_L(\mathbf{a}_S^{approx})) \right\|_{L^2}^2. \quad (18)$$

5 Streamline-Upwind Petrov–Galerkin ROM (SUPG-ROM)

In this section, we present the SUPG-ROM for (1). The SUPG-ROM is obtained by adding a stabilizing term to the G-ROM 2, as follows:

$$a(\mathbf{u}_L, \mathbf{v}_L) = \langle \mathbf{f}, \mathbf{v}_L \rangle + \tau_L \langle Res(\mathbf{u}_L), c \partial_x \mathbf{v}_L \rangle, \quad (19)$$

where τ_L is the so-called ‘‘stabilized coefficient,’’ and $Res(\mathbf{u}_L) = \mathbf{f} - (-\mu\partial_{xx}\mathbf{u}_L + c\partial_x\mathbf{u}_L)$. The matrix-vector form of (19) is

$$(\mathbf{A}_{LL} + \tau_L \mathbf{A}_{supg}) \mathbf{a}_L = \mathbf{b}_L, \quad (20)$$

where the ROM operators \mathbf{A}_{LL} and \mathbf{b}_L were defined right after (2). Furthermore, since we are using a linear FE basis and POD modes that have zero boundary conditions, only the weak form of the convective part does not vanish in the SUPG derivation; in other words, $\mathbf{A}_{supg} = c^2 \mathbf{S}_{LL}$.

We use three different ways to find the optimal τ_L value. First, we use the following two formulas inspired by the FE case in [5]:

$$\tau_L^{M1} = \frac{1}{|c|L}, \quad (21a)$$

$$\tau_L^{M2} = \frac{1}{2|c|L} \left(\coth(Pe) - \frac{1}{Pe} \right), \quad Pe := \frac{|c|}{2\mu L}. \quad (21b)$$

Next, we use a trial and error approach to find the optimal stabilized coefficient. In Figure 1, we list the trial and error plots for different L values. Specifically, we fix an interval for the stabilized coefficient τ_L and randomly choose a candidate for τ_L , and then we compute the SUPG-ROM errors using the metric definitions 24a-24b below. The candidate τ_L value that yields the least SUPG-ROM error is the optimal stabilized coefficient.

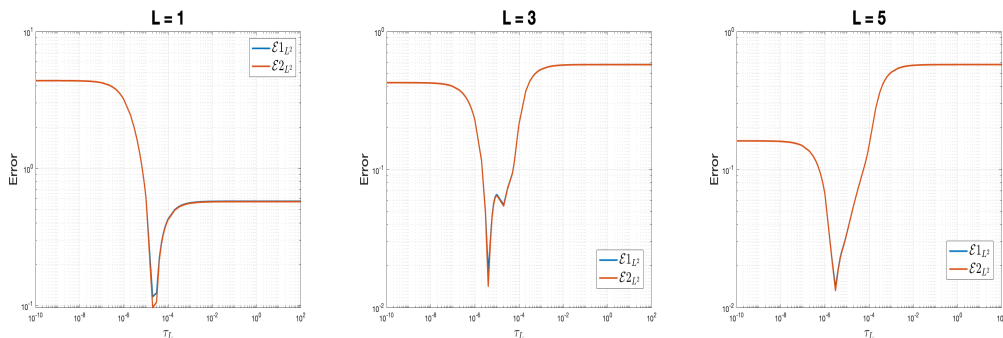


Figure 1: Trial and error plots to find the optimal stabilized coefficient for various L values.

Finally, we use a data-driven approach to find the optimal stabilized coefficient by creating the following ansatz:

$$\mathbf{A}_{LS} \mathbf{a}_S \approx \tau_L \mathbf{A}_{supg} \mathbf{a}_L, \quad (22)$$

where $\tau_L \in \mathbb{R}^{L \times L}$.

6 Numerical Results

In this section, we investigate the numerical accuracy of the coefficient-based and residual-based D2-VMS-ROMs and SUPG-ROMs. Furthermore, we investigate the consistency of the coefficient-based and residual-based D2-VMS-ROMs.

We present numerical results for the parameter-dependent CD problem (1) with the following exact solution, which is used in [14]:

$$u(x, \mu) = \frac{\exp(cx/\mu) - 1}{\exp(c/\mu) - 1} - x, \quad (23)$$

where μ is a parameter. The force term is $f = -c = -400$.

Snapshot Generation We generate the FOM results for $\mu \in [1, 10]$ with $\Delta\mu = 1$ values by using a linear FE spatial discretization with mesh size $h = 1/4096$.

ROM Construction We generate the ROM basis functions and operators by collecting the snapshots, which are the solutions of (1) for $\mu^{training} = 1, 2, \dots, 9, 10$. To build the ROM basis, we use the POD [8, 16]. To train the D2-VMS-ROM operators, $\tilde{\mathbf{A}}$ and $\tilde{\mathbf{b}}$, we use the FOM data for all the $\mu^{training}$ values. We test all the ROMs for $\mu^{testing} = 0.5, 0.1, 0.05, 15$, which fall outside the training range. Thus, we are testing all the ROMs in the *predictive regime*.

To compare the numerical accuracy of the methods, we use two different metrics to compute the ROM errors:

$$\mathcal{E}1_{L^2} = \left\| \mathbf{u}_L(\mu^{testing}) - \mathbf{u}^{FOM}(\mu^{testing}) \right\|_{L^2}, \quad (24a)$$

$$\mathcal{E}2_{L^2} = \left\| \mathbf{u}_L(\mu^{testing}) - \sum_{i=1}^L \left(\mathbf{u}^{FOM}(\mu^{testing}), \boldsymbol{\varphi}_i \right)_{L^2} \boldsymbol{\varphi}_i \right\|_{L^2}. \quad (24b)$$

The metrics (24a) and (24b) measure the error with respect to the FOM solution and the projection of the exact solution on the reduced space, respectively.

6.1 Testing the ROMs for $\mu = 0.5$

In this section, we compare the accuracy of all the ROMs considering the metrics (24a)-(24b) for just one testing parameter value, $\mu = 0.5$, which is outside the training range.

In Tables 1 and 2, we list the ROM errors for all the methods that were introduced in the previous sections, which are run for the testing parameter $\mu = 0.5$ (outside the training range) and assessed using the metrics (24a)-(24b).

L	G	C1	C2	R1a	R1b	R2a	R2b
1	4.38e+00	5.72e+00	6.38e-02	6.37e-02	6.37e-02	6.37e-02	6.37e-02
2	3.72e-01	3.66e-01	2.51e-02	2.49e-02	2.49e-02	2.64e-02	2.55e-02
3	4.26e-01	4.19e-01	1.16e-02	1.15e-02	1.15e-02	1.19e-02	1.19e-02
4	1.68e-01	1.68e-01	6.69e-03	6.55e-03	6.55e-03	6.78e-03	6.79e-03
5	1.61e-01	1.61e-01	4.56e-03	4.45e-03	4.45e-03	4.61e-03	4.61e-03
6	9.92e-02	9.92e-02	3.41e-03	3.33e-03	3.33e-03	3.44e-03	3.44e-03
7	9.49e-02	9.49e-02	2.69e-03	2.63e-03	2.63e-03	2.71e-03	2.71e-03

Table 1: L^2 error (24a) for G-ROM, C-ROMs, R1-ROMs, and R2-ROMs for various L values.

L	G	C1	C2	R1a	R1b	R2a	R2b
1	4.38e+00	5.72e+00	2.84e-03	5.45e-04	5.45e-04	3.04e-04	2.97e-06
2	3.71e-01	3.66e-01	3.53e-03	1.04e-04	1.04e-04	8.88e-03	5.85e-03
3	4.26e-01	4.19e-01	2.06e-03	7.64e-05	8.87e-05	3.14e-03	3.14e-03
4	1.68e-01	1.68e-01	1.38e-03	8.19e-05	8.17e-05	1.78e-03	1.80e-03
5	1.61e-01	1.61e-01	1.00e-03	2.46e-04	2.46e-04	1.22e-03	1.22e-03
6	9.92e-02	9.92e-02	7.59e-04	1.72e-04	1.72e-04	8.84e-04	8.84e-04
7	9.48e-02	9.48e-02	5.95e-04	1.18e-04	1.18e-04	6.80e-04	6.80e-04

Table 2: L^2 error (24b) for G-ROM, C-ROMs, R1-ROMs, and R2-ROMs for various L values.

The errors in Table 2 are equal to or significantly lower than the errors in Table 1. For both Table 1 and 2, the G-ROM and C1-ROM yield the worst results among all the ROMs. Furthermore, R1a and R1b-ROMs give the lowest errors among all the ROMs. In Table 1, the R1a and R1b and R2a and R2b-ROM errors are almost the same. Thus, there is no interest in adding the term $\tilde{\mathbf{b}}$ to the residual-based ansatzes. In view of the smallest errors achieved with the metric (24b), to differentiate the accuracy of the models, from now on, we use only that metric.

In Table 2, we observe that as L goes to d , the R1a and R1b and R2a and R2b errors are similar. In other words, the data-driven operator $\tilde{\mathbf{b}}$ goes to zero, confirming that it does not have a significant effect on the numerical accuracy. Thus, to list the errors, from now on, we use only R1a and R2a among the four R-D2-VMS-ROMs. Moreover, since C2-ROM yields more accurate results than C1-ROM, to make a fair comparison among all ROMs, we list C2-ROM as well.

In Tables 3 and 4, we list the SUPG-ROM errors by using different τ_L values and the metrics (24a)-(24b). The SUPG-ROM with $\tau_L^{trial-training}$ minimizes the following quantity:

$$\sum_{j=1}^{10} \left(\mathbf{u}_L(\tau^{trial-training}) - \mathbf{u}^{FOM}(\tau_j) \right)^2 \quad (25)$$

The optimal $\tau_L^{trial-testing}$ corresponds to the lowest SUPG-ROM error with respect to the metric (24b) for the testing parameter $\mu^{testing} = 0.5$. In the last column, the SUPG-ROM errors are calculated by modeling the τ_L term with a data-driven approach. Overall, the errors in Table 4 are lower than the errors in Table 3. Thus, from now on, we use metric (24b) to list the SUPG-ROM errors. For both Tables 3 and 4, the second and third columns (i.e., τ_L^{M1} and τ_L^{M2} , which are calculated by using (21a)-(21b)), give the highest SUPG-ROM errors. In Tables 3 and 4, among all SUPG-ROMs with different τ_L models, $\tau_r^{trial-testing}$ one yields the lowest error. Thus, in what follows, we compute the SUPG-ROM errors only considering the $\tau_r^{trial-testing}$ model.

L	τ_L^{M1}	τ_L^{M2}	$\tau_L^{trial-training}$	$\tau_L^{trial-testing}$	τ_L^{d2}
1	5.70e-01	5.63e-01	1.23e-01	1.16e-01	5.72e+00
2	5.51e-01	5.27e-01	8.35e-02	3.11e-02	4.54e-01
3	5.23e-01	4.72e-01	5.56e-02	1.83e-02	4.86e-01
4	4.86e-01	4.00e-01	7.06e-02	1.59e-02	1.70e-01
5	4.40e-01	3.22e-01	7.06e-02	1.40e-02	1.61e-01
6	3.89e-01	2.53e-01	7.05e-02	1.40e-02	9.92e-02
7	3.38e-01	2.05e-01	7.05e-02	1.36e-02	9.49e-02

Table 3: L^2 error (24a) for SUPG-ROM with various τ_L models and L values.

In Tables 5, 6, and 7, to investigate the ROM consistency, we list the norm of the closure term and its ansatz. For example, in Table 5, we investigate the consistency behavior of the C-D2-VMS-ROMs, i.e., C1-ROM and C2-ROM. Since the closure term is the same for both models, we list the norm of the closure term, $\mathbf{A}_{LS} \mathbf{a}_S$, and the C1-ROM, C2-ROM errors for all L values. Based on the numerical results, we observe that the C2-ROM error has the same order of magnitude as the closure term, whereas the order of magnitude of the C1-ROM error quickly diminishes. Thus, we conclude that C2-ROM is a more consistent model than C1-ROM. We perform the same consistency investigation for R1-D2-VMS-ROMs and R2-D2-VMS-ROMs. In Tables 6-7, we list the norm of the

L	τ_L^{M1}	τ_L^{M2}	$\tau_L^{trial-training}$	$\tau_L^{trial-testing}$	τ_L^{d2}
1	5.66e-01	5.60e-01	1.05e-01	9.64e-02	5.72e+00
2	5.51e-01	5.26e-01	7.97e-02	1.87e-02	4.54e-01
3	5.23e-01	4.72e-01	5.44e-02	1.42e-02	4.86e-01
4	4.86e-01	4.00e-01	7.02e-02	1.45e-02	1.69e-01
5	4.40e-01	3.22e-01	7.05e-02	1.33e-02	1.61e-01
6	3.89e-01	2.53e-01	7.04e-02	1.36e-02	9.92e-02
7	3.38e-01	2.05e-01	7.04e-02	1.33e-02	9.48e-02

Table 4: L^2 error (24b) for SUPG-ROM with various τ_L models and L values.

closure terms, \mathbf{a}_S and $\mathbf{Res}_L(\mathbf{a}_S)$, and the R1a, R1b, and R2a, R2b errors, respectively. In both tables, we observe that the order of magnitude of the R1-ROMs and R2-ROMs are the same as their closure terms, and as L goes to d , R1a and R1b, and R2a and R2b-ROMs yield the same results. Thus, we conclude that R1-ROMs and R2-ROMs are equally consistent models.

L	$\mathbf{A}_{LS} \mathbf{a}_S$	C1	C2	L	$\mathbf{A}_{LS} \mathbf{a}_S$	C1	C2
1	3.06e+02	7.10e+02	3.08e+02	6	5.90e+02	2.40e-02	8.70e+02
2	1.21e+03	1.77e+01	1.22e+03	7	4.18e+02	9.31e-05	7.77e+02
3	1.21e+03	1.90e+01	1.26e+03	8	2.64e+02	7.84e-05	7.00e+02
4	1.00e+03	7.06e-01	1.12e+03	9	1.26e+02	1.02e-02	6.36e+02
5	7.85e+02	3.76e-01	9.85e+02	10	0	0	0

Table 5: Consistency error comparison for C-D2-VMS-ROMs with various L values.

L	\mathbf{a}_S	R1a	R1b	L	\mathbf{a}_S	R1a	R1b
1	6.37e-02	7.01e-02	7.01e-02	6	2.95e-03	6.03e-03	6.03e-03
2	2.48e-02	2.67e-02	2.67e-02	7	2.13e-03	5.12e-03	5.12e-03
3	1.14e-02	1.28e-02	1.36e-02	8	1.50e-03	7.41e-04	7.41e-04
4	6.36e-03	8.77e-03	8.77e-03	9	9.35e-04	4.23e-04	4.23e-04
5	4.17e-03	7.11e-03	7.10e-03	10	0	0	0

Table 6: Consistency error comparison for R1-D2-VMS-ROM with various L values.

L	$\mathbf{Res}_L(\mathbf{a}_S)$	R2a	R2b	L	$\mathbf{Res}_L(\mathbf{a}_S)$	R2a	R2b
1	4.24e+01	4.07e+01	4.64e+01	6	6.86e+02	9.31e+02	9.31e+02
2	1.24e+03	1.32e+03	1.25e+03	7	5.31e+02	8.24e+02	8.24e+02
3	1.21e+03	1.23e+03	1.23e+03	8	4.43e+02	6.97e+03	3.60e+02
4	1.06e+03	1.16e+03	1.16e+03	9	3.74e+02	3.57e+02	3.57e+02
5	8.34e+02	1.00e+03	1.00e+03	10	0	0	0

Table 7: Consistency error comparison for R2-D2-VMS-ROM with various L values.

6.2 Testing for All μ Values

Instead of further investigating different $\mu^{testing}$ values that are out of the training set, we use the average L^2 error (26) to measure the ROM consistency for $\mu^{testing} = 0.5, 0.1, 0.05, 15$.

$$\mathcal{E}_{avg} = \frac{1}{M} \sum_{j=1}^M \left\| \mathbf{u}_L(\mu_j^{testing}) - \sum_{i=1}^r \left(\mathbf{u}^{FOM}(\mu_j^{testing}), \boldsymbol{\varphi}_i \right)_{L^2} \boldsymbol{\varphi}_i \right\|_{L^2}. \quad (26)$$

In Table 8, we list the average L^2 errors for G-ROM, C-ROM (C2-ROM, which is a more consistent model than the C1-ROM), R1-ROM (R1a-ROM, which yields the same results as R1b-ROM as L goes to d , but because R1a-ROM does not contain the extra data-driven operator, $\tilde{\mathbf{b}}$, R1a-ROM is more consistent than R1b-ROM), R2-ROM (R2a-ROM, same explanation holds for this case), and SUPG-ROM (SUPG-ROM considering $\tau_L^{trial-testing}$ model). In what follows, we denote C2-ROM, R1a-ROM, and R2a-ROM as C-ROM, R1-ROM, and R2-ROM, respectively.

L	G-ROM	C-ROM	R1-ROM	R2-ROM	SUPG-ROM
1	1.95e+01	3.99e-03	8.98e-04	1.14e-03	1.47e-01
2	4.17e-01	5.76e-03	2.11e-04	1.13e-02	7.07e-02
3	3.31e+00	5.06e-03	2.92e-04	6.24e-03	4.57e-02
4	3.07e-01	4.68e-03	3.36e-04	5.36e-03	3.11e-02
5	1.93e+00	4.43e-03	1.03e-03	4.91e-03	2.30e-02
6	2.64e-01	4.17e-03	8.30e-04	4.53e-03	1.90e-02
7	1.49e+00	3.95e-03	6.54e-04	4.25e-03	1.67e-02

Table 8: Average L^2 error (26) for G-ROM, C-ROM, R1-ROM, R2-ROM, and SUPG-ROM for various L values.

Based on the errors in Table 8, G-ROM and R1-ROM are the least and most accurate, respectively. SUPG-ROM is more accurate than G-ROM and less accurate than C-ROM, R1-ROM, and R2-ROM. Finally, although R2-ROM involves more information from the sub-scale equation, R1-ROM is more accurate than R2-ROM.

7 Conclusions

In this paper, we investigated data-driven ROM closure modeling for convection-dominated problems. Specifically, we considered three types of ROM closure modeling using available data to construct accurate ROM closure operators. The first type of data-driven ROM closure that we investigated was the standard coefficient-based D2-VMS-ROM (C-D2-VMS-ROM) [12, 17]. The second type of data-driven ROM closure was a novel residual-based D2-VMS-ROM (R-D2-VMS-ROM), in which the closure term is a function of the ROM residual. We also investigated an SUPG-ROM stabilization strategy in which the stabilization parameter was computed either by extrapolating the classical FE scalings or by using data-driven modeling. Finally, for comparison purposes, we investigated a standard G-ROM in which stabilization and closure were not used. We investigated the new R-D2-VMS-ROM and the standard C-D2-VMS-ROM, SUPG-ROM, and G-ROM in the numerical simulation of a one-dimensional parameter-dependent convection-diffusion problem in the predictive regime (i.e., for parameters that were not used in the training stage).

Our numerical investigation yielded the following conclusions: First, the novel R-D2-VMS-ROM was the most accurate model. Second, R-D2-VMS-ROM was more consistent than the standard C-D2-VMS-ROM. Third, R-D2-VMS-ROM, C-D2-VMS-ROM, and SUPG-ROM were more accurate than G-ROM. Finally, the SUPG-ROM version with the data-driven stabilization parameter was more accurate than the SUPG-ROM with the FE extrapolated stabilization parameter.

There are several research directions that can be pursued next. Probably the most important is the extension of the new R-D2-VMS-ROM framework to more complex convection-dominated problems, such as under-resolved turbulent flows.

Acknowledgments: Research partially funded by Programma Operativo FEDER Andalusia 2014-2020 grant US-1254587, ARIA MSCA-RISE EU Grant 872442, and National Science Foundation grant DMS- 2012253.

References

- [1] S. E. Ahmed, S. Pawar, O. San, A. Rasheed, T. Iliescu, and B. R. Noack. On closures for reduced order models – a spectrum of first-principle to machine-learned avenues. *Phys. Fluids*, 33(9):091301, 2021.
- [2] M. Bergmann, C. H. Bruneau, and A. Iollo. Enablers for robust POD models. *J. Comput. Phys.*, 228(2):516–538, 2009.
- [3] A. N. Brooks and T. J. R. Hughes. Streamline upwind/Petrov-Galerkin formulations for convection dominated flows with particular emphasis on the incompressible Navier-Stokes equations. *Computer methods in applied mechanics and engineering*, 32(1):199–259, 1982.
- [4] A. Caiazzo, T. Iliescu, V. John, and S. Schyschlowa. A numerical investigation of velocity-pressure reduced order models for incompressible flows. *J. Comput. Phys.*, 259:598–616, 2014.
- [5] I. Christie, D. F. Griffiths, A. R. Mitchell, and O. C. Zienkiewicz. Finite element methods for second order differential equations with significant first derivatives. *International Journal for Numerical Methods in Engineering*, 10(6):1389–1396, 1976.
- [6] M. Couplet, P. Sagaut, and C. Basdevant. Intermodal energy transfers in a proper orthogonal decomposition–Galerkin representation of a turbulent separated flow. *J. Fluid Mech.*, 491:275–284, 2003.
- [7] S. Giere, T. Iliescu, V. John, and D. Wells. SUPG reduced order models for convection-dominated convection-diffusion-reaction equations. *Comput. Methods Appl. Mech. Engrg.*, 289:454–474, 2015.
- [8] P. Holmes, J. L. Lumley, and G. Berkooz. *Turbulence, Coherent Structures, Dynamical Systems and Symmetry*. Cambridge, 1996.
- [9] T. Iliescu and Z. Wang. Variational multiscale proper orthogonal decomposition: Convection-dominated convection-diffusion-reaction equations. *Math. Comput.*, 82(283):1357–1378, 2013.

- [10] T. Iliescu and Z. Wang. Variational multiscale proper orthogonal decomposition: Navier-Stokes equations. *Num. Meth. P.D.E.s*, 30(2):641–663, 2014.
- [11] B. Kragel. *Streamline diffusion POD models in optimization*. PhD thesis, Universität Trier, 2005.
- [12] C. Mou, B. Koc, O. San, L. G. Rebholz, and T. Iliescu. Data-driven variational multiscale reduced order models. *Computer Methods in Applied Mechanics and Engineering*, 373:113470, 2021.
- [13] P. Pacciarini and G. Rozza. Stabilized reduced basis method for parametrized advection–diffusion PDEs. *Comput. Meth. Appl. Mech. Eng.*, 274:1–18, 2014.
- [14] T. C. Rebollo and B. M. Dia. A variational multi-scale method with spectral approximation of the sub-scales: Application to the 1D advection–diffusion equations. *Computer Methods in Applied Mechanics and Engineering*, 285:406–426, 2015.
- [15] R. Reyes and R. Codina. Projection-based reduced order models for flow problems: A variational multiscale approach. *Comput. Methods Appl. Mech. Engrg.*, 363:112844, 2020.
- [16] S. Volkwein. Proper orthogonal decomposition: Theory and reduced-order modelling. *Lecture Notes, University of Konstanz*, 2013. <http://www.math.uni-konstanz.de/numerik/personen/volkwein/teaching/POD-Book.pdf>.
- [17] X. Xie, M. Mohebujjaman, L. G. Rebholz, and T. Iliescu. Data-driven filtered reduced order modeling of fluid flows. *SIAM J. Sci. Comput.*, 40(3):B834–B857, 2018.